Biochem. J. (2011) **439**, 215–225 (Printed in Great Britain) doi:10.1042/BJ20110753



# Crystal structures and kinetic studies of human Kappa class glutathione transferase provide insights into the catalytic mechanism

Bing WANG*†, Yingjie PENG*[1], Tianlong ZHANG* and Jianping DING*[2]

*State Key Laboratory of Molecular Biology and Research Center for Structural Biology, Institute of Biochemistry and Cell Biology, Shanghai Institutes for Biological Sciences, Chinese Academy of Sciences, Shanghai 200031, China, and †Graduate School of Chinese Academy of Sciences, 320 Yue-Yang Road, Shanghai 200031, China

GSTs (glutathione transferases) are a family of enzymes that primarily catalyse nucleophilic addition of the thiol of GSH (reduced glutathione) to a variety of hydrophobic electrophiles in the cellular detoxification of cytotoxic and genotoxic compounds. GSTks (Kappa class GSTs) are a distinct class because of their unique cellular localization, function and structure. In the present paper we report the crystal structures of hGSTk (human GSTk) in apo-form and in complex with GTX (*S*-hexylglutathione) and steady-state kinetic studies, revealing insights into the catalytic mechanism of hGSTk and other GSTks. Substrate binding induces a conformational change of the active site from an 'open' conformation in the apo-form to a 'closed' conformation in the GTX-bound complex, facilitating formations of the G site (GSH-binding site) and the H site (hydrophobic substrate-binding site). The conserved $Ser^{16}$ at the G site functions as the catalytic residue in the deprotonation of the thiol group and the conserved $Asp^{69}$, $Ser^{200}$, $Asp^{201}$ and $Arg^{202}$ form a network of interactions with $\gamma$-glutamyl carboxylate to stabilize the thiolate anion. The H site is a large hydrophobic pocket with conformational flexibility to allow the binding of different hydrophobic substrates. The kinetic mechanism of hGSTk conforms to a rapid equilibrium random sequential Bi Bi model.

Key words: catalytic mechanism, conformational change, crystal structure, Kappa class glutathione transferase (GSTk), kinetic measurement, substrate-binding pocket.

## INTRODUCTION

GSTs (glutathione transferases) are a family of multifunctional enzymes that play important roles primarily in the cellular detoxification of cytotoxic and genotoxic compounds. The main chemistry of GSTs is to catalyse nucleophilic addition of the thiol group of GSH (reduced glutathione), the tripeptide $\gamma$-Glu-Cys-Gly, to a wide variety of hydrophobic electrophiles [1–6]. The products of the conjugation are more soluble non-toxic peptide derivatives. GSTs exist in all eukaryotes as well as in many bacteria, which have been divided into a number of classes based on their amino acid sequence homology in combination with other criteria, including tertiary structure similarity, substrate specificity and immunological properties [1,6–8]. Although GSTs share less than 30 % identity among different classes, almost all canonical GSTs (also called soluble or cytosolic GSTs) function as dimers. The residues forming the G site (GSH-binding site) are highly conserved, whereas the residues forming the H site (hydrophobic substrate-binding site) are less conserved to allow a wide range of substrate selectivity. In addition to their function in cellular detoxification, GSTs are implicated to play important roles in cell signalling and other cellular processes [9–11], and are associated with many human diseases [12–16].

On the basis of structural and biochemical studies of several classes of soluble GSTs, in particular the Alpha, Mu and Pi classes of GSTs, the catalytic mechanism of nucleophilic aromatic substitution reaction by GSTs has been postulated to consist of four steps: (i) substrate binding to the active site, (ii) activation of GSH by thiol deprotonation to form the thiolate anion, (iii) nucleophilic attack of the thiolate on the electrophilic centre of the substrate to form a thioether bond, and (iv) release of the resulting product [1,17–20]. The activation of GSH to form the thiolate anion is the critical step in the catalytic reaction. It is proposed that a conserved residue at the active site (tyrosine in Alpha, Mu and Pi classes, serine in Theta and Delta classes, and cysteine in the Omega class) facilitates the thiol deprotonation by forming a hydrogen bond with the thiol group of GSH [19,21–23]. It is also proposed that the $\gamma$-glutamyl carboxylate group of GSH functions as the catalytic base to accept the proton from the thiol group of GSH, and an electron-sharing network helps to stabilize the thiolate anion [20,24,25].

GSTks (Kappa class GSTs) are suggested to form a distinct family of the Trx (thioredoxin)-fold superfamily, different from the soluble GSTs [5,26–29]. They localize in the matrix of mitochondria and peroxisomes of the cells, and exhibit a GSH-dependent conjugation activity with model substrates [26,28,30], and possibly other activities including peroxidase and isomerase [27,29]. The structure of rGSTk (rat mitochondrial GSTk) in complex with GSH demonstrated that the enzyme is structurally more similar to DsbA than to the soluble GSTs, suggesting that it was evolved in a parallel pathway from that of the soluble GSTs [23,29,31]. DsbA is a protein disulfide oxidoreductase that catalyses the formation of disulfide bonds in *Escherichia coli*. It was reported that overexpression of GSTk in mouse cells up-regulates the multimerization of adiponectin molecules, probably through formation of intracellular disulfide bonds [32]. However, GSTks do not contain a conserved CXXC motif at the active site which is required by DsbA to catalyse the oxidation and

Abbreviations used: CDNB, 1-chloro-2,4-dinitrobenzene; DTT, dithiothreitol; GSDNB, *S*-(2,4-dinitrophenyl)glutathione; GSF, glutathione sulfinate; GSH, reduced glutathione; G site, GSH-binding site; GST, glutathione transferase; GSTk, Kappa class GST; GTX, *S*-hexylglutathione; HCCA, 2-hydroxychromene-2-carboxylic acid; hGSTk, human GSTk; H site, hydrophobic substrate-binding site; PEG, poly(ethylene glycol); rGSTk, rat GSTk; RMSD, root mean square deviation; Trx, thioredoxin.

[1] Present address: Department of Molecular Biology, The Scripps Research Institute, 10550 North Torrey Pines Road, La Jolla, CA 92037, U.S.A.
[2] To whom correspondence should be addressed (email jpding@sibs.ac.cn).

The structures of hGSTk in apo-form and in complex with GTX have been deposited with the RCSB PDB under accession codes 3RPP and 3RPN respectively.

isomerization of disulfide bonds in substrate proteins [33,34], and thus are unlikely to catalyse a DsbA-type reaction. The structure of hGSTk (human GSTk) in complex with GSF (glutathione sulfinate) showed that hGSTk has a similar overall structure to that of rGSTk and its Trx-fold domain is structurally more similar to that of human Theta class GST than the other soluble GSTs, although the two enzymes share a very low sequence identity (19 %) [35]. In addition, the active site of both rGSTk and hGSTk is similar to that of the soluble GSTs, and GSTks appear to function in a manner similar to that of the soluble GSTs [23].

To understand the catalytic mechanism of GSTks, we carried out structural and biochemical studies of hGSTk. In the present paper we report the crystal structures of hGSTk in apo-form and in complex with an inhibitor, namely GTX (*S*-hexylglutathione), and the mutagenesis and steady-state kinetic studies of the enzyme. The structural and biochemical data taken together reveal that hGSTk utilizes an induced-fit mechanism for substrate binding and a rapid equilibrium random sequential Bi Bi kinetic mechanism for catalysis, and suggest that other GSTks might function in a similar manner.

## MATERIALS AND METHODS

### Protein expression and purification

The hGSTk protein was expressed in *E. coli* and purified by affinity chromatography using a nickel-chelating resin, as described previously [35]. The purified protein was dialysed against buffer containing 20 mM $NaH_2PO_4$ (pH 7.4), 20 mM NaCl, 1 mM EDTA and 1 mM DTT (dithiothreitol) for biochemical studies. The protein used for crystallization of the apo-form of hGSTk was dialysed against buffer containing 20 mM $NaH_2PO_4$ (pH 7.4), 20 mM NaCl, 1 mM EDTA and 7.2 mM 2-mercaptoethanol. The protein used for crystallization of hGSTk in complex with GTX was dialysed against buffer containing 20 mM Hepes (pH 7.0), 50 mM NaCl, 1 mM EDTA and 1 mM DTT. Constructs of the hGSTk mutants containing point mutations were generated using the QuikChange® Site-Directed Mutagenesis kit (Stratagene) and were verified by DNA sequencing. The procedures for expression and purification of the mutants were the same as those for the wild-type protein.

### Crystallization and diffraction data collection

Crystals of the apo-form of hGSTk were grown by the hanging drop vapour diffusion method at 4 °C in drops containing equal volumes (0.5 $\mu$l) of the protein solution (5 mg/ml) and the crystallization solution {0.2 M $Mg(NO_3)_2$ and 15 % PEG [poly(ethylene glycol)] 3350}. Crystals of hGSTk in complex with GTX were grown by the hanging drop vapour diffusion method at 20 °C in drops containing equal volumes (0.5 $\mu$l) of the protein solution (10 mg/ml) supplemented with GTX (Sigma) at a molar ratio of 1:2 and the crystallization solution (0.2 M NaSCN and 20 % PEG3350). Diffraction data of the apo-form and GTX-bound hGSTk were collected to 1.80 Å (1 Å = 0.1 nm) and 1.90 Å resolution respectively, at 100 K from flash-cooled crystals at the Shanghai Synchrotron Radiation Facility, Shanghai, China, and processed using the HKL2000 suite [36]. The diffraction data statistics are summarized in Table 1.

### Structure determination and refinement

Crystal structures of both the apo-form and GTX-bound hGSTk were solved using the molecular replacement method implemented in the program MOLREP [37] with the structure of hGSTk in complex with GSF (PDB code 1YZX) [35] as the search model. The initial structure refinement was carried out with the program CNS [38] following the standard protocols, and the final structure refinement was performed using the program PHENIX [39]. No non-crystallographic symmetry constraint was applied in the refinement. The manual model building was performed with the program COOT [40]. In the initial difference Fourier maps, there was strong electron density corresponding to a GTX molecule in each hGSTk subunit in the hGSTk–GTX complex. The statistics of the structure refinements and the final structure models are summarized in Table 1. The quality of the stereochemistry of the structure models was validated with the program PROCHECK [41]. The molecular graphic images were prepared using the program PyMOL (http://www.pymol.org).

**Table 1 Summary of diffraction data and structure refinement statistics**

Numbers in parentheses indicate the highest resolution shell.

| Measurement | hGSTk | hGSTk-GTX |
|---|---|---|
| Diffraction data | | |
| Space group | *C*2 | $P2_1$ |
| Cell parameters | | |
| *a*, *b*, *c* (Å) | 146.1, 84.3, 87.3 | 66.4, 199.8, 66.7 |
| $\alpha, \beta, \gamma$ (°) | 90.0, 122.1, 90.0 | 90.0, 116.1, 90.0 |
| Resolution (Å) | 50.0–1.80 (1.86–1.80) | 50.0–1.90 (1.97–1.90) |
| Observed reflections | 511931 | 413733 |
| Unique reflections [$I/\sigma(I)>0$] | 82817 | 116840 |
| Average $I/\sigma(I)$ | 21.6 (4.9) | 19.7 (3.6) |
| Completeness (%) | 100.0 (100.0) | 95.8 (98.7) |
| $R_{merge}$ (%)* | 10.0 (23.5) | 9.8 (32.7) |
| Refinement and structure model | | |
| Reflections [$F_o \geqslant 0\sigma(F_o)$] | | |
| Working set | 78674 | 110664 |
| Test set | 4142 | 5836 |
| *R* factor (%)† | 15.2 | 18.3 |
| Free *R* factor (%)† | 19.5 | 21.8 |
| Number of non-hydrogen atoms | 5914 | 11418 |
| Number of amino acid residues | 649 | 1320 |
| Number of water molecules | 752 | 804 |
| Average *B* factor (Å$^2$) | | |
| All atoms | 27.6 | 38.9 |
| Protein | 26.3 | 38.1 |
| GTX | – | 45.2 |
| Water molecules | 36.7 | 47.1 |
| RMSDs | | |
| Bond lengths (Å) | 0.006 | 0.007 |
| Bond angles (°) | 0.954 | 0.989 |
| Ramachandran plot (%) | | |
| Most favoured regions | 92.4 | 91.5 |
| Allowed regions | 7.6 | 8.5 |

*$R_{merge} = \sum_{hkl} \sum_i |I_i(hkl) - \langle I(hkl)\rangle| / \sum_{hkl} \sum_i I_i(hkl)$.
†$R_{factor} = \sum_{hkl} ||F_o| - |F_c|| / \sum_{hkl} |F_o|$.

### Enzymatic activity assay and kinetic analysis

The enzymatic activity assay of both wild-type and mutant hGSTk catalysing the addition of GSH to CDNB (1-chloro-2,4-dinitrobenzene) was carried out using a modified protocol, as described previously [31]. All steady-state kinetic experiments were performed in buffer containing 20 mM $NaH_2PO_4$ (pH 7.4), 20 mM NaCl, 1 mM EDTA and 1 mM DTT at 25 °C, and the amount of the product was measured at 338 nm using a Beckman Coulter DU800 spectrophotometer. The enzymatic reaction rate was linear up to 60 s after initiation and the initial rate was measured at 2 s intervals for a total period of 60 s. The non-enzymatic reaction rate served as a control and was subtracted from the enzymatic rate. Owing to the low solubility of CDNB in water, ethanol was used as the solvent for CDNB. To avoid a

**Table 2 Steady-state kinetic parameters of wild-type and mutant hGSTk containing point mutation at the G site towards GSH**

The kinetic parameters are the means ± S.D. of triplicate determinations. ND means that the enzymatic activity is too low to be detected.

| hGSTk | $K_m^{GSH}$ (mM) | $k_{cat}$ ($s^{-1}$) | $k_{cat}/K_m$ ($M^{-1}\cdot s^{-1}$) |
|---|---|---|---|
| Wild-type | 0.19 ± 0.02 | 1.18 ± 0.02 | (6.21 ± 0.52)×10$^3$ |
| S16A | 17.34 ± 4.79 | 0.17 ± 0.03 | 9.80 ± 3.20 |
| Y18F | 20.45 ± 3.53 | 1.56 ± 0.10 | (7.63 ± 1.40)×10 |
| Y18H | ND | ND | |
| Y18L | ND | ND | |
| Y18A | ND | ND | |
| S19A | 1.61 ± 0.41 | 3.74 ± 0.51 | (2.32 ± 0.67)×10$^3$ |
| N53A | 4.53 ± 0.38 | 1.75 ± 0.05 | (3.86 ± 0.34)×10$^2$ |
| P56A | 1.68 ± 0.31 | 2.29 ± 0.16 | (1.36 ± 0.27)×10$^3$ |
| K62A | 1.25 ± 0.07 | 0.89 ± 0.01 | (7.12 ± 0.39)×10$^2$ |
| K62E | 25.26 ± 3.89 | 0.75 ± 0.04 | (2.97 ± 0.48)×10 |
| D69T | 60.89 ± 13.66 | 1.33 ± 0.11 | (2.18 ± 0.52)×10 |
| D69A | 105.39 ± 21.83 | 0.32 ± 0.04 | 3.04 ± 0.74 |
| L183A | 9.81 ± 1.75 | 0.47 ± 0.03 | (4.79 ± 0.90)×10 |
| S200A | 1.03 ± 0.19 | 0.99 ± 0.06 | (9.61 ± 1.88)×10$^2$ |
| D201A | 4.74 ± 1.08 | 0.47 ± 0.01 | (9.92 ± 2.26)×10 |
| R202A | 123.60 ± 74.89 | 0.67 ± 0.20 | 5.42 ± 3.63 |

**Table 3 Steady-state kinetic parameters of wild-type and mutant hGSTk containing point mutation at the H site towards CDNB**

The kinetic parameters are the means ± S.D. of triplicate determinations. ND means that the enzymatic activity is too low to be detected.

| hGSTk | $K_m^{CDNB}$ (mM) | $k_{cat}$ ($s^{-1}$) | $k_{cat}/K_m$ ($M^{-1}\cdot s^{-1}$) |
|---|---|---|---|
| Wild-type | 1.10 ± 0.12 | 3.94 ± 0.23 | (3.58 ± 0.45)×10$^3$ |
| L15A | 2.59 ± 0.43 | 1.19 ± 0.18 | (7.37 ± 1.41)×10$^2$ |
| P17A | 0.34 ± 0.04 | 2.38 ± 0.11 | (7.00 ± 0.85)×10$^3$ |
| I44A | 2.01 ± 0.44 | 3.28 ± 0.46 | (1.63 ± 0.42)×10$^3$ |
| P55A | 1.08 ± 0.14 | 4.50 ± 0.28 | (4.17 ± 0.60)×10$^3$ |
| P56A | 0.74 ± 0.07 | 7.83 ± 0.40 | (1.06 ± 0.12)×10$^4$ |
| L58A | 1.45 ± 0.16 | 2.40 ± 0.14 | (1.66 ± 0.21)×10$^3$ |
| M66A | >5 | ND | |
| F83A | 1.30 ± 0.16 | 6.24 ± 0.44 | (4.80 ± 0.68)×10$^3$ |
| F83W | 0.64 ± 0.07 | 3.18 ± 0.15 | (4.97 ± 0.61)×10$^3$ |
| F87A | 0.91 ± 0.10 | 4.18 ± 0.22 | (4.59 ± 0.55)×10$^3$ |
| F87W | 1.38 ± 0.17 | 5.78 ± 0.41 | (4.19 ± 0.59)×10$^3$ |
| L88A | 4.44 ± 0.74 | 5.00 ± 0.58 | (1.13 ± 0.23)×10$^3$ |
| M91A | 0.62 ± 0.05 | 5.50 ± 0.20 | (8.87 ± 0.80)×10$^3$ |
| M91K | 0.63 ± 0.07 | 5.11 ± 0.24 | (8.11 ± 0.96)×10$^3$ |
| L92A | >5 | ND | |
| W126A | 0.17 ± 0.02 | 2.94 ± 0.09 | (1.73 ± 0.16)×10$^4$ |

potential effect of ethanol on the enzymatic activity, the ethanol concentration was adjusted to 5 % (v/v) in both the activity assay system and the control system. All experiments were repeated three times under the same conditions.

To measure the effect of mutations on the binding of GSH, the reaction mixture consisted of a constant concentration of CDNB (0.5 mM, Sigma) and various concentrations of GSH (0.05–200 mM, Sigma). To measure the effect of mutations on the binding of CDNB, the reaction mixture consisted of a constant concentration of GSH (1 mM) and various concentrations of CDNB (0.05–5 mM). The apparent kinetic parameters $K_m$ and $k_{cat}$ (Tables 2 and 3) were determined by fitting the kinetic data to the Michaelis–Menten equation using non-linear regression analysis implemented in the program Prism 4.0 (GraphPad Software).

To calculate the initial velocity of the enzymatic reaction, the kinetic data were fitted to eqn (1) for the rapid equilibrium random sequential Bi Bi model [42,43] according to Scheme 1.

$$v = \frac{V_{max}[GSH][CDNB]}{\alpha K_d^{GSH} K_d^{CDNB} + \alpha K_d^{GSH}[CDNB] + \alpha K_d^{CDNB}[GSH] + [GSH][CDNB]} \quad (1)$$

where $v$ is the initial velocity of the enzymatic reaction, $\alpha$ is the coupling factor, $K_d^{GSH}$ is the dissociation constant of GSH, and $K_d^{CDNB}$ is the dissociation constant of CDNB (dissociation constants of hGSTk for GSH and CDNB: $K_d^{GSH}$ 0.16 ± 0.04 mM, $K_d^{CDNB}$ 1.23 ± 0.59 mM, $\alpha$ 0.51 ± 0.04). Inhibition studies were carried out in a similar manner as for the initial velocity studies using GSDNB [*S*-(2,4-dinitrophenyl)glutathione] (provided by the Xu laboratory, Shanghai University, Shanghai, China) as the product inhibitor. The inhibitor was fixed at several concentrations ranging from 0 to 66.7 $\mu$M. The parameters of the rate equation were obtained from the Lineweaver–Burk plots and the secondary plots that were constructed as described previously [44].

## RESULTS

### Overall structures of the apo-form and GTX-bound hGSTk

The crystal structure of the apo-form of hGSTk was refined to 1.80 Å resolution, yielding an *R* factor of 0.152 and a free *R* factor of 0.195 (Table 1). There are three hGSTk molecules in an asymmetric unit with two molecules forming a dimer and the third forming a dimer with a two-fold crystallographic axis-related molecule. The crystal structure of hGSTk in complex with GTX was refined to 1.90 Å resolution, yielding an *R* factor of 0.183 and a free *R* factor of 0.218 (Table 1). There are six hGSTk molecules in an asymmetric unit forming three dimers and each hGSTk is bound with a GTX molecule at the active site. No significant conformational difference exists among the three hGSTk molecules in the apo-form and the six hGSTk molecules in the GTX-bound complex [the RMSD (root mean square deviation) values are approximately 0.2 Å and 0.3 Å respectively]. GTX is an inhibitor of GSTs with a hexyl group that conjugates to the thiol group of GSH. In the structure of the hGSTk–GTX complex, there was strong electron density without ambiguity for the GSH moiety of GTX with an identical conformation at the active site of each subunit. However, the hexyl group of GTX has two distinct conformations in the two subunits of the dimer with well-defined electron density and occupies part of the H site. Consistently, the average *B* factor of the hexyl group of GTX (68.4 Å$^2$) is much higher than that of the GSH moiety of GTX (38.3 Å$^2$) and that of the protein (38.1 Å$^2$), indicating a high flexibility of the hexyl group.

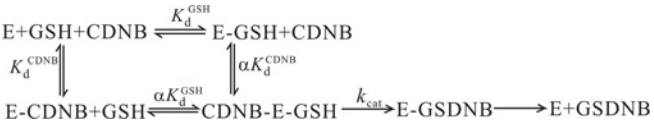


**Scheme 1 The conjugation reaction of GSH and CDNB catalysed by hGSTk**

The overall structure of hGSTk in the apo-form and the GTX-bound complex is very similar to that in the GSF-bound complex [35] with an RMSD of <0.48 Å for 204 C$\alpha$ atoms between the apo-form and the GSF-bound complex, and <0.70 Å for 217 C$\alpha$ atoms between the GTX-bound and GSF-bound complexes. hGSTk consists of a Trx-fold domain and an $\alpha$-helical domain (Figures 1A and 1B). The Trx-fold domain (domain I) is composed of a $\beta\alpha\beta\alpha$ ($\beta1\alpha1\beta2\alpha2$) motif and a $\beta\beta\alpha$ ($\beta3\beta4\alpha10$) motif

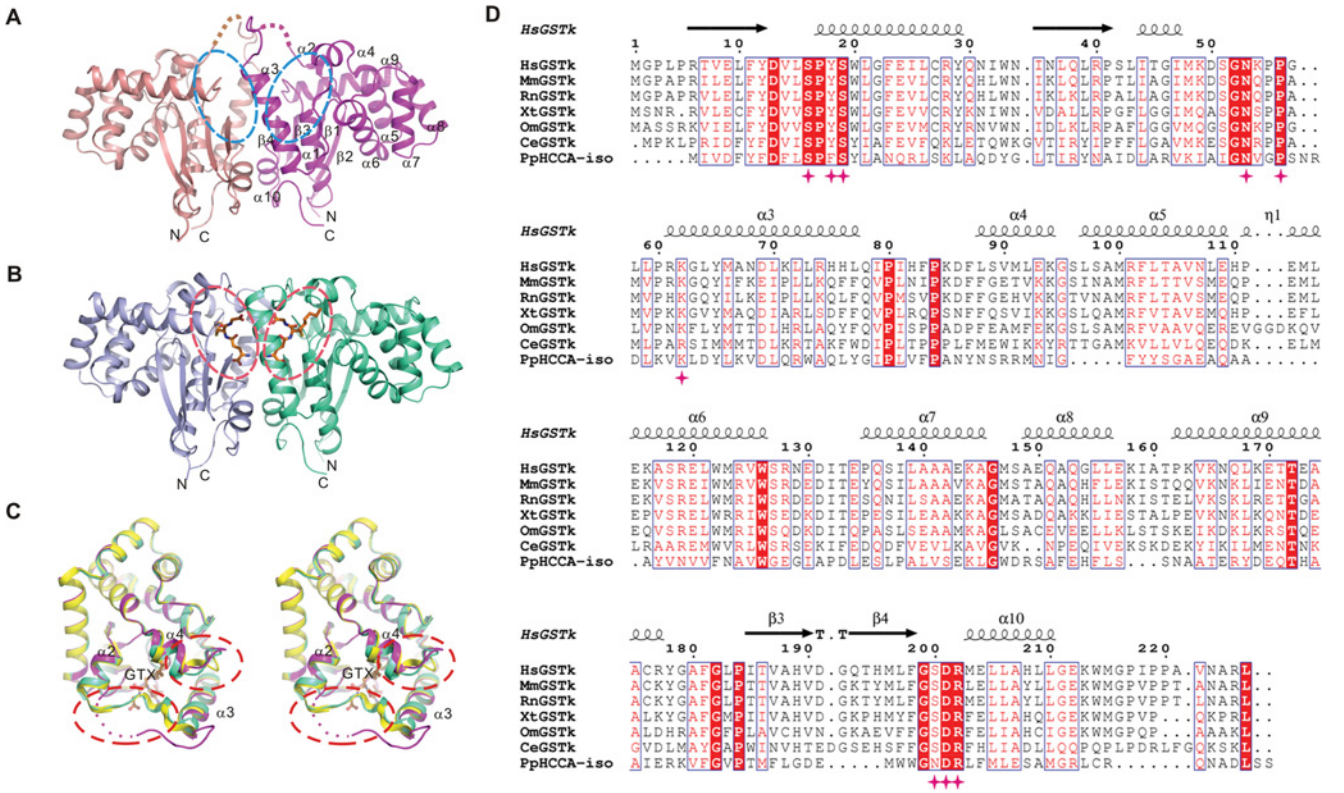


**Figure 1 Overall structures of hGSTk**

(**A**) Overall structure of the apo-form of hGSTk. The disordered regions of residues Asp[50]–Gly[52] are indicated with dotted lines. The active sites are circled with dashed lines. (**B**) Overall structure of the hGSTk–GTX complex. The bound GTX molecules are shown as ball-and-stick models. The active sites are circled with dashed lines. (**C**) Superimposition of the monomers of three hGSTk structures. The apo-form of hGSTk is shown in pink, the GTX-bound hGSTk is in green, and the GSF-bound hGSTk is in yellow (PDB code 1YZX). The disordered region of residues Asp[50]–Gly[52] in the apo-form hGSTk structure is indicated with a dotted line. The bound GTX molecule is shown as a ball-and-stick model. The regions with substantial conformational differences are circled with dashed lines. (**D**) Sequence alignment of GSTks from different species. The alignment was generated by ESPript [51] with the secondary structures of hGSTk at the top of the alignment. The conserved residues forming the G site are marked with red stars. HsGSTk, *Homo sapiens* GSTk1; MmGSTk, *Mus musculus* GSTk1; RnGSTk, *Rattus norvegicus* GSTk1; XtGSTk, *Xenopus tropicalis* GSTk1; OmGSTk, *Oncorhynchus mykiss* GSTk1; CeGSTk, *Caenorhabditis elegans* GSTk1; and PpHCCA-iso, *Pseudomonas putida* HCCA isomerase.

forming a four-stranded $\beta$-sheet surrounded by three $\alpha$-helices. The $\alpha$-helical domain (domain II) is composed of seven $\alpha$-helices ($\alpha$3–$\alpha$9), and is inserted between the N-terminal $\beta\alpha\beta\alpha$ motif and the C-terminal $\beta\beta\alpha$ motif of the Trx-fold domain. This domain topology is similar to that of rGSTk, but different from that of the soluble GSTs in which the Trx-fold domain and the $\alpha$-helical domain are linked together contiguously. The dimeric hGSTk has an open-wings butterfly shape which is also different from the canonical globular shape of the soluble GSTs. The dimer interface is dominated by hydrophobic interactions between residues of domain I of one subunit and domain II of the other. As in most of the soluble GSTs, the conserved Pro[184] at the N-terminal $\beta$3 adopts a *cis*-conformation. Previous studies have shown that the conserved *cis*-proline residue in the soluble GSTs plays an important role in maintaining the conformational stability of the active site [45,46].

The major conformational differences between the apo-form and the GTX-bound hGSTk occur at the active site, in particular the $\alpha$2–$\alpha$3 loop (residues Ile[46]–Arg[61]) which forms part of the G and H sites, and the $\alpha$3–$\alpha$4 loop (residues Ile[81]–Val[90]) which forms part of the H site (Figure 1C). In the hGSTk–GTX complex which is similar to the hGSTk–GSF complex, residues Asn[53]–Pro[60] form a surface-exposed loop with the region of residues Pro[55]–Leu[59] forming a short $3_{10}$ $\alpha$-helix, and several residues of this region including Asn[53] and Pro[56], and a residue from the other subunit, namely Lys[62′] (residues of the adjacent subunit are denoted with a prime) are involved in direct interactions with the GSH moiety of GTX (see the results and discussion below). In the apo-form of hGSTk, residues Asp[50]–Gly[52] are disordered and the flanking regions (Met[48]–Lys[49] and Asn[53]–Lys[54]) exhibit higher *B* factors. Furthermore, residues Pro[55]–Leu[59] form a loop and are positioned away from the G site (the C$\alpha$ atom of Pro[56] in the apo-form of hGSTk is displaced by approximately 14 Å away from that in the GSF/GTX-bound hGSTk). In the hGSTk–GTX complex, the $\alpha$3–$\alpha$4 loop assumes different conformations in the two subunits to accommodate the hexyl group of GTX with different conformations, both of which are slightly different from those in the apo-form of hGSTk and the hGSTk–GSF complex (see the results and discussion below). These results suggest that the G and H sites have conformational flexibilities and the substrate binding induces conformational changes at the active site.

## Structure of the G site

The G site of hGSTk resides in a hydrophilic cleft at the dimer interface and is formed by structural elements of both subunits, including helices $\alpha$1 and $\alpha$3 and the $\beta$4–$\alpha$10 loop of domain I, and the two connecting loops between domain I and domain II (the $\alpha$2–$\alpha$3 and $\alpha$9–$\beta$3 loops) of one subunit, and helix $\alpha$3 and the $\beta$4–$\alpha$10 loop of the other subunit (Figures 1A and 1B). This is slightly different from the soluble GSTs in which the G site is located in a cleft between domain I of one subunit and domain

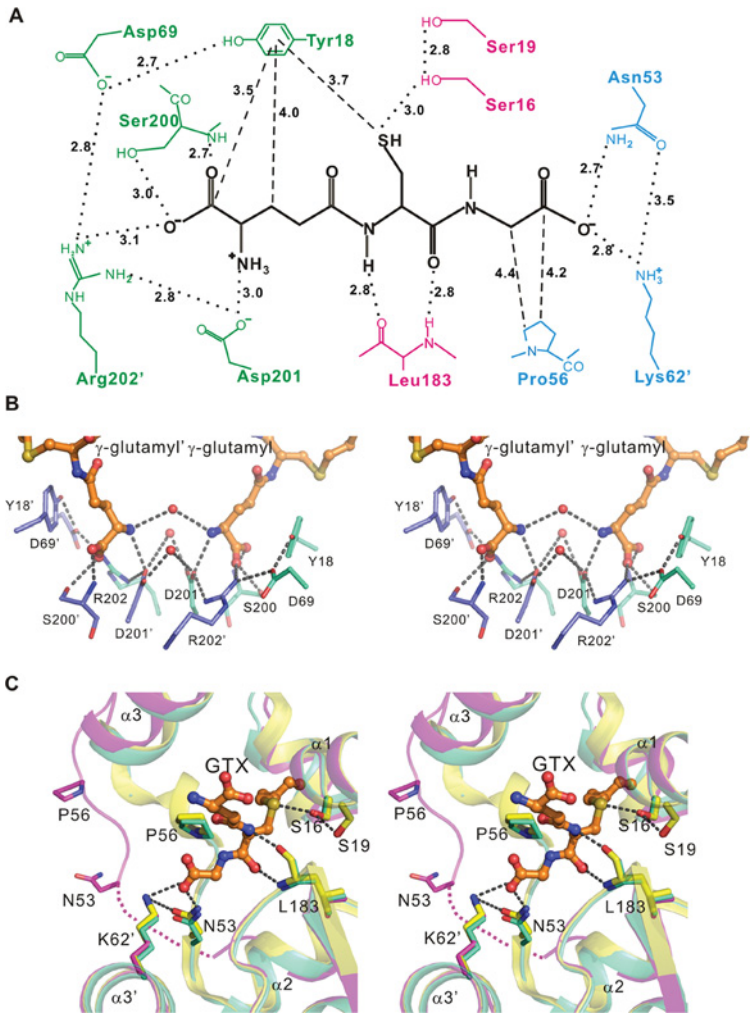


**Figure 2 Structure of the G site**

(**A**) Schematic diagram showing the interactions of the GSH moiety of GTX with the surrounding residues in the hGSTk–GTX complex. The salt bridges and hydrogen bonds are shown as dotted lines, and the hydrophobic interactions are shown as dashed lines. The distances (in Å) of the interactions are indicated. (**B**) A detailed view of the interactions between the two $\gamma$-glutamyl moieties of GTX at the adjacent G sites in the hGSTk–GTX complex. The $\gamma$-glutamyl moiety of GTX is shown as a ball-and-stick model, and the main chain of Ser$^{200}$ and the side chains of Tyr$^{18}$, Asp$^{69}$, Ser$^{200}$, Asp$^{201}$ and Arg$^{202}$ are shown as stick models. Three water molecules are shown as red spheres. The network of hydrogen bonds and salt bridges are indicated with dotted lines. (**C**) Structural comparison of the G site of hGSTk in the apo-form (pink), the GTX-bound complex (green) and the GSF-bound complex (yellow). The disordered region of residues Asp$^{50}$–Gly$^{52}$ in the apo-form of hGSTk is indicated with a pink dotted line. GTX is shown as a ball-and-stick model, and the side chains of Ser$^{16}$, Ser$^{19}$, Asn$^{53}$, Pro$^{56}$, Lys$^{62'}$ and Leu$^{183}$, and the main chain of Leu$^{183}$ are shown as stick models. The hydrogen-bonding and salt bridge interactions are indicated with dotted lines.

II of the other, and residues of domain I provide the interactions for the specific recognition of GSH [1,17–19]. In the hGSTk–GTX complex, the GSH moiety of GTX maintains interactions with several conserved residues of hGSTk (Figure 2A), similar to those in the hGSTk–GSF complex [35], and most of the interactions are also conserved in the rGSTk–GSH complex [31]. Specifically, the $\gamma$-glutamyl moiety of GSH is mainly recognized by the conserved strand-turn-helix motif (the $\beta$4–$\alpha$10 loop) consisting of Ser$^{200}$, Asp$^{201}$ and Arg$^{202'}$ (Figures 2A and 2B). The $\gamma$-glutamyl carboxylate group makes a salt bridge with the side-chain amino of Arg$^{202'}$ (3.1 Å) and two hydrogen bonds with the main-chain amide (2.7 Å) and the side-chain hydroxy group (3.0 Å) of Ser$^{200}$ respectively, and the $\gamma$-glutamyl amino group makes a salt bridge with the side-chain carboxyl group of Asp$^{201}$ (3.0 Å). The positively charged side chain of Arg$^{202'}$ also forms two salt bridges with the negatively charged side chains of Asp$^{201}$ and Asp$^{69}$ (2.8 Å for both). The side chain of Asp$^{69}$ makes another hydrogen bond with the side-chain hydroxy group of Tyr$^{18}$ (2.7 Å). Meanwhile, the phenolic ring of Tyr$^{18}$ forms hydrophobic contacts with the $\gamma$-glutamyl moiety and the thiol group of GSH. Additionally, there are three water molecules at the dimer interface to mediate the interactions between the two $\gamma$-glutamyl moieties of the adjacent subunits (Figure 2B). To investigate the functional roles of these residues in catalysis, we performed mutagenesis and steady-state kinetics studies (Table 2). Mutation R202A resulted in a significantly increased $K_m$ of GSH (661-fold) and a slightly decreased $k_{cat}$ (1.8-fold), and mutation D201A resulted in a moderately increased $K_m$ of GSH (25-fold) and a slightly decreased $k_{cat}$ (2.5-fold). Mutation S200A had relatively less profound effects on the $K_m$ of GSH (increased 5.5-fold) and the $k_{cat}$ (decreased 1.2-fold) than mutations D201A and R202A. Replacement of Asp$^{69}$ by alanine resulted in a 564-fold increase in the $K_m$ of GSH and a 3.7-fold decrease in the $k_{cat}$, and that by threonine resulted in a 326-fold increase in the $K_m$ of GSH, but had no appreciable effect on the $k_{cat}$. These results indicate that the conserved residues Asp$^{69}$, Ser$^{200}$, Asp$^{201}$

and Arg[202] play very important roles in the binding of GSH, but less profound roles in catalysis through stabilization of the γ-glutamyl moiety of GSH. Surprisingly, mutation of Tyr[18] to alanine, leucine or histidine led to undetected binding of GSH and enzymatic activity, and mutation of Tyr[18] to phenylalanine yielded a markedly increased $K_m$ of GSH (109-fold), but had a slightly increased $k_{cat}$ (1.3-fold), indicating that Tyr[18] plays critical roles in both GSH binding and catalysis. It is possible that Tyr[18] is not only involved in stabilization of the γ-glutamyl carboxylate of GSH via the hydrogen-bonding interaction with Asp[69], but also in precise positioning and/or correct orientation of the thiol group and the γ-glutamyl moiety of GSH via hydrophobic interactions.

As in the soluble GSTs and rGSTk, the sulfur atom of the cysteinyl moiety of GSH is recognized via a hydrogen bond (3.0 Å) by the side-chain hydroxy group of Ser[16] at the N-terminus of α1, which is further stabilized via a hydrogen bond by the side-chain hydroxy group of Ser[19] (2.8 Å) (Figures 2A and 2C). Additionally, the main-chain amino and carbonyl groups of the cysteinyl moiety form two hydrogen bonds with the main-chain carbonyl and amino groups of Leu[183] at the α9–β3 loop (2.8 Å for both). The equivalent of Ser[16] in rGSTk and the soluble GSTs was proposed to act as a catalytic residue in the ionization of the thiol group of GSH [19,21–23,31]. The functional roles of Ser[16] and the other residues in catalysis are confirmed by mutagenesis and steady-state kinetic studies (Table 2). The biochemical data show that mutation S16A caused a greatly increased $K_m$ of GSH (93-fold) and a markedly decreased $k_{cat}$ (6.9-fold), mutation S19A resulted in a slightly increased $K_m$ of GSH (8.6-fold) but a moderately increased $k_{cat}$ (3.2-fold), and mutation L183A caused a 53-fold increase in the $K_m$ of GSH and a 2.5-fold decrease in the $k_{cat}$. These results support the notion that the conserved Ser[16] plays a critical role in catalysis. Structural comparison shows that all of these residues and the structural elements interacting with the cysteinyl moiety of GSH maintain similar conformations in the apo-form and GSF/GTX-bound hGSTk, indicating that the proposed catalytic residue maintains a stable conformation in the substrate binding.

The carboxylate of the glycyl moiety of GSH makes a hydrogen bond with the side-chain amide of Asn[53] (2.7 Å) and the main chain of the glycyl moiety makes hydrophobic contacts with the side chain of Pro[56] (Figures 2A and 2C). The biochemical data show that mutation N53A resulted in a 24-fold increase in the $K_m$ of GSH and a 1.5-fold increase in the $k_{cat}$, and mutation P56A yielded a 9-fold increase in the $K_m$ of GSH and a 1.9-fold increase in the $k_{cat}$ (Table 2). Since mutations of Asn[53] and Pro[56], both of which are located in the α2–α3 connecting loop that undergoes conformational change upon the GTX/GSF binding, have much less effect on the $K_m$ of GSH than the residues that are involved in interactions with the γ-glutamyl and cysteinyl moieties of GSH, these results suggest that the α2–α3 loop is involved in the binding of GSH, but plays a less critical role than the residues interacting with the γ-glutamyl and cysteinyl moieties. Previously it was reported that the soluble GSTs contain a functionally conserved basic residue (histidine, lysine or arginine) at the active site that interacts directly with the glycyl carboxylate of GSH and plays an important role in GSH binding and catalysis [47]. In the hGSTk–GTX complex, the side-chain amino group of Lys[62′] makes a salt bridge with the carboxylate of the glycyl moiety of GSH (2.8 Å) as well as a hydrogen bond with the side-chain carbonyl of Asn[53] (3.5 Å) (Figures 2A and 2C). Mutation of Lys[62] to glutamate or alanine increased the $K_m$ of GSH 135-fold or 7-fold, but had a minor effect on the $k_{cat}$ (reduced 1.6- or 1.3-fold) (Table 2). These results indicate that Lys[62′] of hGSTk plays a similar functional role in the binding of GSH to that of the conserved basic residue of the soluble GSTs.

### Structure of the H site

Owing to the lack of a hydrophobic substrate-bound GSTk structure, the exact binding site for the hydrophobic substrate in GSTk is not well defined. In the hGSTk–GTX complex, there is a large hydrophobic pocket near the G site, and the hexyl group of GTX occupies part of the pocket with distinct conformations in the two subunits of the dimer and the two conformers differ by 70°: in subunit A, the hexyl group has hydrophobic contacts with the side chains of Leu[15], Pro[17], Met[66], Leu[88], Met[91] and Leu[92]; in subunit B, the hexyl group has hydrophobic contacts with the side chains of Pro[17], Tyr[18], Met[66], Phe[83], Leu[88] and Trp[126], and the main chain of Ala[67] (Figure 3A). Concurrently, the α3–α4 loop assumes different conformations in the two subunits which are also different from those in the apo-form and GSF-bound hGSTk structures (Figure 1C). Compared with that in subunit A, the α3–α4 loop in subunit B shifts towards helix α3 with the Cα atom of Lys[85] in the middle of the loop displaced by 4.5 Å. In addition, Phe[83], Phe[87] and Met[91] assume different side-chain conformations to accommodate the hexyl group of GTX with different conformations.

To better understand the binding site of the hydrophobic substrate in hGSTk, we docked a GSDNB molecule, the conjugation product of GSH and CDNB, into the active site of hGSTk based on the position of the GSH moiety of GTX or GSF. GSDNB can be docked into the active site of hGSTk in both the apo-form and the GTX/GSF-bound complex, and particularly the CDNB moiety of GSDNB can be accommodated into the large hydrophobic pocket without obvious steric conflict with the protein (Figures 3B and 3C). On the basis of the modelling studies, the H site of hGSTk can be defined as a large hydrophobic pocket composed of Leu[15]–Tyr[18] of the β1–α1 loop and Ile[44] of helix α2 of domain I, Met[66] of helix α3, Leu[88]–Leu[92] of the α3-α4 loop, and Trp[126] of helix α6 of domain II, and Pro[55]–Leu[58] of the α2–α3 loop which links domain I and domain II (Figure 3B). This is also slightly different from the soluble GSTs in which the H site is mainly formed by the structural elements of domain II [1,17–19]. Owing to the conformational differences of the α3–α4 loop and the hexyl group of GTX in the two subunits of the hGSTk–GTX complex, the CDNB moiety of GSDNB can be docked into the H site in two slightly differed conformations (Figure 3B). This implies that the shape and size of the H site in hGSTk may vary to some extent to bind different hydrophobic substrates. The kinetic data show that mutations of the residues forming the H site had various effects on the hydrophobic substrate binding but insignificant effects on the $k_{cat}$ (Table 3). Specifically, mutations of Leu[15], Ile[44], Met[66], Leu[88] and Leu[92] which make close hydrophobic interactions with the CDNB moiety of GSDNB and undergo conformational changes upon the binding of GTX or GSF, had relatively large effects on the $K_m$ of CDNB (increased approximately 2–5-fold), probably because of the loss of favourable hydrophobic contacts. Mutations of Pro[17] and Trp[126], which also make close hydrophobic interactions with the CDNB moiety but have no conformational change upon the substrate binding, yielded a markedly decreased $K_m$ of CDNB (approximately 3–6-fold), probably because these mutations might render the H site more flexible and/or more spacious to accommodate the hydrophobic substrate. The other residues, including Pro[55], Pro[56], Leu[58], Phe[83], Phe[87] and Met[91], have less or indirect interactions with the CDNB moiety, and their mutations had minor effects on the $K_m$ of CDNB (<2 fold).

### Kinetic analysis of the catalytic reaction

Previously it was proposed that the catalytic reaction of rGSTk utilizes a rapid equilibrium ordered mechanism with GSH binding

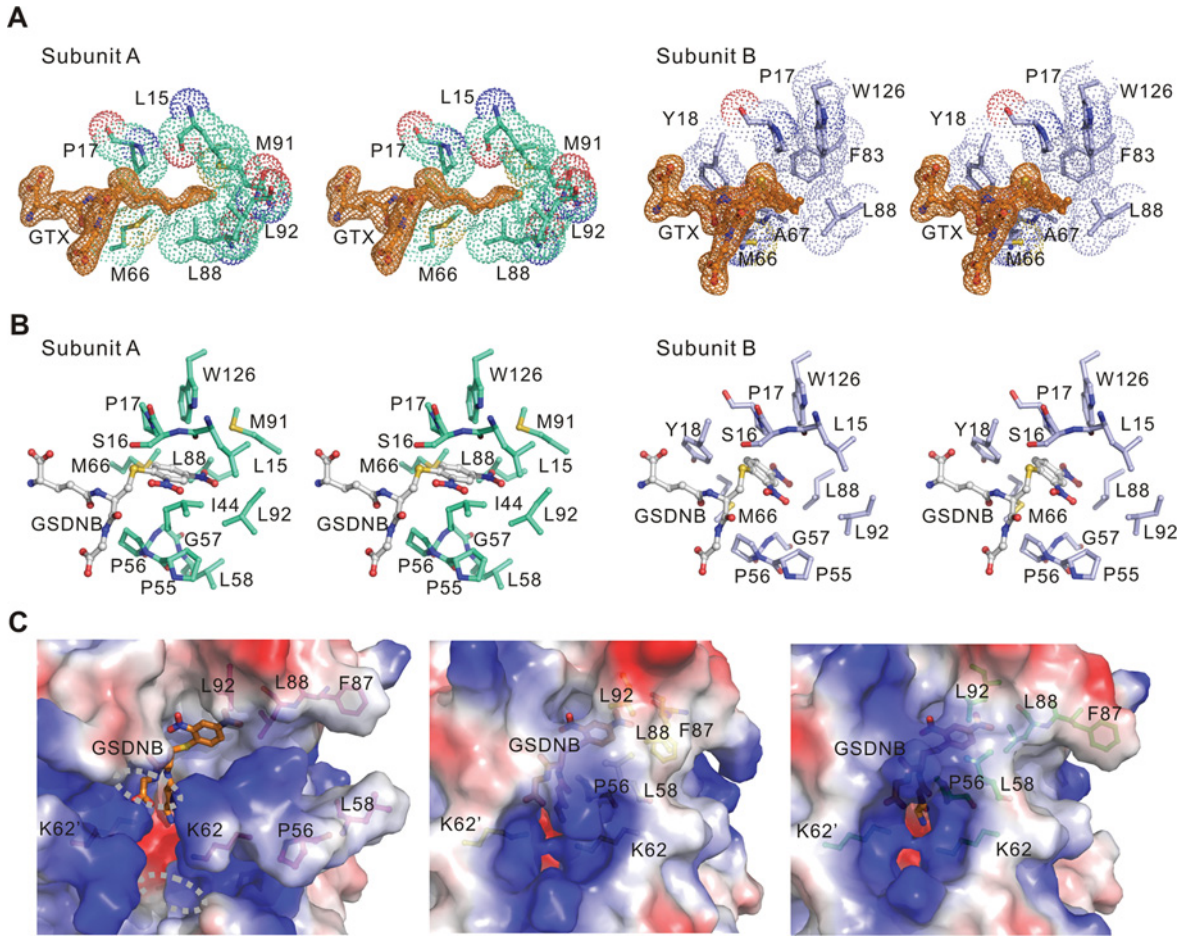


**Figure 3 Structure of the H site**

(**A**) A detailed view showing that the hexyl group of GTX assumes different conformations in the two subunits of the hGSTk–GTX complex. The GTX molecules are covered with a representative SIGMAA-weighted $2F_o - F_c$ map ($1\sigma$ contour level). The residues that have hydrophobic interactions with the hexyl group of GTX are shown as stick models and covered with the van der Waals surfaces. (**B**) Structure of the H site showing the interactions of the docked GSDNB with the surrounding residues in the hGSTk–GTX complex. Owing to the conformational differences of the hexyl group of GTX in the two subunits, the CDNB moiety of GSDNB can be docked into the H site in two slightly different conformations. (**C**) Electrostatic surfaces of hGSTk in the apo-form (left-hand panel), the GSF-bound complex (middle panel) and the GTX-bound complex (right-hand panel) showing the structure of the H site. The disordered regions of residues $Asp^{50}$–$Gly^{52}$ in the apo-form are indicated with dotted circles. The docked GSDNB molecule at the H site is shown in yellow. Some residues of the active site are shown as stick models for reference.

first which induces conformational changes at the active site to facilitate CDNB binding [31]. To gain insights into the kinetic mechanism of hGSTk, we carried out steady-state kinetic studies using GSH and CDNB as the substrates. When GSH was used as the variable substrate and CDNB was used at fixed concentrations, the intersecting point of the Lineweaver–Burk plots is above the horizontal axis, indicating that the apparent $K_m$ of CDNB decreases as the GSH concentration increases (Figure 4A). A similar pattern was obtained when CDNB was used as the variable substrate and GSH at fixed concentrations (Figure 4B). These intersecting initial velocity patterns indicate that the kinetics of hGSTk are consistent with a sequential mechanism with both substrates binding to the enzyme before the product is released [44]. However, as the curvatures of the reciprocal plots of the Lineweaver–Burk plots are too small, it is difficult to fit the kinetic data to a steady-state random sequential Bi Bi model or a steady-state ordered sequential Bi Bi model. To resolve the issue on the binding order of the two substrates, we further performed the inhibition studies with the product GSDNB. The results show that GSDNB exhibits a competitive inhibition and a mixed-type inhibition towards GSH and CDNB respectively (Figures 4C and 4D). The $K_i$ for GSH is $65.9 \pm 3.2\ \mu M$ and $111.9 \pm 28.9\ \mu M$ at the CDNB concentration of 0.5 mM and 1 mM respectively. These data suggest that the kinetic mechanism of hGSTk conforms to the rapid equilibrium random sequential Bi Bi model [44]. The random binding of GSH and CDNB has a coupling factor $\alpha$ of $0.51 \pm 0.04$, indicating that the affinity for CDNB increases in the presence of GSH approximately 2-fold and vice versa ($K_d^{GSH}$ is $0.16 \pm 0.04$ mM, and $K_d^{CDNB}$ is $1.23 \pm 0.59$ mM, $\alpha$ $0.51 \pm 0.04$). Nevertheless, hGSTk binds GSH much more tightly than CDNB as the dissociation constant $K_d^{CDNB}$ is much higher than $K_d^{GSH}$. The coupling of the random binding of GSH and CDNB also implies the existence of an intra-subunit communication between the G and H sites. These kinetic data are supported, in part, by the structural data that in the apo-form of hGSTk both G and H sites are accessible to the solvent to allow the random binding of the substrates, and the binding of GSH at the G site induces conformational changes of the $\alpha 2$–$\alpha 3$ and $\alpha 3$–$\alpha 4$ loops to facilitate the formation of the H site and presumably the binding of CDNB. We expect that the binding of CDNB at the H site would also induce conformational changes of the $\alpha 2$–$\alpha 3$ and $\alpha 3$–$\alpha 4$ loops to facilitate the formation of the G site and the

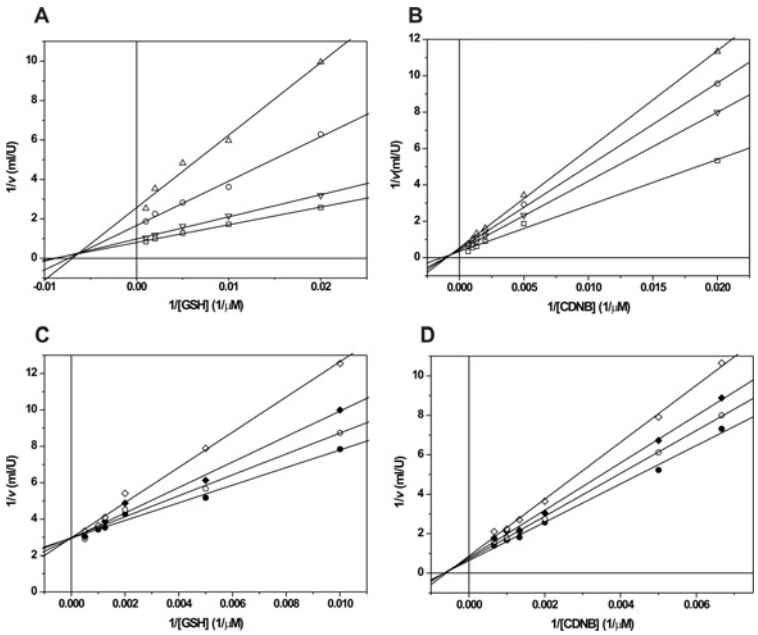


**Figure 4 Steady-state kinetics and inhibition analysis of hGSTk**

(**A**) Initial velocity analysis with GSH at various concentrations and CDNB at fixed concentrations: 0.2 (△), 0.5 (○), 0.75 (▽) and 1.0 (□) mM. (**B**) Initial velocity analysis with CDNB at various concentrations and GSH at fixed concentrations: 0.5 (△), 0.75 (○), 1.5 (▽) and 2.0 (□) mM. (**C**) Lineweaver–Burk plots for the inhibition of hGSTk by product GSDNB at different concentrations of GSH. (**D**) Lineweaver–Burk plots for the inhibition of hGSTk by product GSDNB at different concentrations of CDNB. The assays were performed in the absence or presence of different concentrations of GSDNB: 0 (●), 13.3 (○), 33.4 (◆) and 66.7 (◇) $\mu$M.

binding of GSH. The crystal structure of hGSTk in complex with CDNB is needed to address this issue.

## DISCUSSION

GSTks constitute a distinct family of the Trx-fold superfamily, different from the soluble GSTs in both function and catalytic mechanism [5,26–29]. The previous structural studies of rGSTk and hGSTk have revealed some unique structural features of GSTks. We determined the crystal structures of hGSTk in the apo-form and in complex with GTX and carried out mutagenesis and steady-state kinetic studies of hGSTk. The structural and biochemical data taken together provide new insights into the catalytic mechanism of hGSTk and the other GSTks.

In the conjugation reaction catalysed by the soluble GSTs, the ionization of GSH to form the thiolate anion is an essential step. Previous structural and biochemical studies of the soluble GSTs have led to the proposal of two GSH activation models. The active-site catalytic residue model suggests that a conserved residue (tyrosine in Alpha, Mu and Pi classes, serine in Theta and Delta classes, and cysteine in the Omega class) at the active site functions as a base to receive the proton from the thiol group of GSH and stabilizes the thiolate anion via a hydrogen bond [19,21–23]. Alternatively, the base-assisted deprotonation model suggests that the $\gamma$-glutamyl carboxylate of GSH acts as a base to accept the proton from the thiol group of GSH, which is assisted by a network of hydrophilic interactions to share the negative charge of the $\gamma$-glutamyl carboxylate and to stabilize the thiolate anion [20,24,25]. The proposed electron-sharing network is characterized by electrostatic interactions between the $\gamma$-glutamyl carboxylate, a positively charged residue (primarily arginine), and a negatively charged residue (primarily glutamate or aspartate), which are further stabilized by an array of hydrogen bonds mediated by surrounding residues (serine and threonine) and water molecules. The residues contributing to the electron-sharing network are not conserved in the primary sequence, but are structurally and functionally conserved in most of the soluble GSTs including the Alpha, Pi, Theta and Delta classes [25]. Previously, a molecular dynamics simulation study further suggested that a water molecule at the active site acts as a bridge to assist the transfer of the proton from the thiol group to the $\gamma$-glutamyl carboxylate of GSH after an initial conformational rearrangement of GSH [17].

hGSTk contains a strictly conserved $Ser^{16}$ at the active site which forms a hydrogen bond with the sulfur atom of GTX in the GTX-bound or GSF in the GSF-bound complex (Figures 1D and 2A). In addition, hGSTk also contains a strictly conserved SDR motif which forms a network of salt bridges and hydrogen bonds with the $\gamma$-glutamyl carboxylate of GSH (Figures 1D and 2A). In the hGSTk–GTX and hGSTk–GSF complexes, the $\gamma$-glutamyl carboxylate of GSH forms an electrostatic interaction with the positively charged $Arg^{202'}$ which makes two electrostatic interactions with the negatively charged $Asp^{201}$ and $Asp^{69}$ (Figure 2B). These interactions are further stabilized by a network of hydrogen bonds involving $Tyr^{18}$, $Ser^{200}$ and three water molecules. Our mutagenesis data show that mutations of $Ser^{16}$ and the residues involved in the formation of the interaction network with the $\gamma$-glutamyl carboxylate have significant effects on the binding of GSH and the $k_{cat}$, underscoring their functional importance in catalysis (Table 2). However, mutation of $Ser^{16}$ that makes a direct hydrogen bond with the thiol group of GSH has the most significant effect on the $k_{cat}$ than the other residues, and mutations of the residues that are involved in salt-bridge interactions with the $\gamma$-glutamyl carboxylate of GSH have the most significant effects on the binding of GSH than the other residues. Furthermore, the structural data show that the $\gamma$-glutamyl carboxylate of GSH is positioned >8 Å away from the

thiol group, suggesting that it is unlikely to be involved directly or indirectly via a water molecule in the deprotonation of the thiol group. Thus our structural and biochemical data together support the active-site catalytic residue model for the GSH activation in which $Ser^{16}$ functions as the catalytic base in thiol deprotonation, and the $\gamma$-glutamyl carboxylate of GSH plays an important role in stabilizing the deprotonated thiolate anion rather than functioning as a catalytic base. The network of interactions involving $Asp^{69}$, $Ser^{200}$, $Asp^{201}$, $Arg^{202}$ and water molecules help to stabilize the negatively charged $\gamma$-glutamyl carboxylate of GSH. In addition, the strictly conserved $Tyr^{18}$ also plays an important role in catalysis through stabilization and precise positioning of the $\gamma$-glutamyl carboxylate and the thiol group of GSH.

Structural comparison of the apo-form and the GTX- and GSF-bound hGSTk reveals that substrate binding induces substantial conformational changes of the active site from an 'open' conformation to a 'closed' conformation. In particular, the $\alpha2$–$\alpha3$ loop which constitutes part of the G and H sites assumes a partially disordered loop structure and is positioned away from the active site in the apo-form of hGSTk, but adopts an ordered loop structure and interacts directly with the GSH moiety of GSF or GTX in the substrate-bound complexes. The kinetic data confirm that the key residues of this region, including $Asn^{53}$, $Pro^{56}$ and $Lys^{62}$, play important roles in the binding of GSH and in catalysis. In addition, the $\alpha3$–$\alpha4$ loop which constitutes part of the H site also assumes different conformations among different hGSTk structures, and is involved in the binding of the hexyl group of GTX. The kinetic data also confirm that the key residues of this region, particularly $Leu^{88}$ and $Leu^{92}$, are involved in the binding of the hydrophobic substrate. In addition, the structural data show that the G and H sites are coupled together via a shared structural element (the $\alpha2$–$\alpha3$ loop), and the conformational change at one site upon the binding of one substrate could induce conformational change of the other site to facilitate the binding of the other substrate. This is consistent with the kinetic data showing that hGSTk utilizes a rapid equilibrium random sequential Bi Bi mechanism, and the random binding of GSH and CDNB are coupled together with a coupling factor of 0.51. Although conformational changes of the active site upon substrate binding have been observed in some classes of the soluble GSTs [43,48], the conformational change of the $\alpha2$–$\alpha3$ loop at the active site of hGSTk upon substrate binding is unique as this loop connects domains I and II and forms part of the G and H sites. The large conformational changes of both G and H sites in hGSTk might be beneficial to the enzyme to be able to bind a wide range of substrates, including the canonical hydrophobic substrates and potential protein substrates.

In the apo-form of hGSTk, the active site assumes an 'open' conformation, and both the G and H sites are accessible to the solvent allowing the random binding of the substrates (Figure 3C). In the GTX- or GSF-bound hGSTk, the binding of GTX or GSF renders the enzyme a 'closed' active site owing to the conformational changes of the $\alpha2$–$\alpha3$ and $\alpha3$–$\alpha4$ loops, and the H site is inaccessible to the solvent even though it is only partially occupied or unoccupied (Figure 3C). The 'closed' H site in the GTX- or GSF-bound hGSTk structure appears to be in disagreement with the proposed kinetic mechanism of random sequential binding of GSH and CDNB. However, our structural data also show that the $\alpha3$–$\alpha4$ loop in both the GSF- and GTX-bound complexes exhibits relatively high *B* factors, indicating a high flexibility of this region even in the presence of GSH. Thus we propose that the binding of GSH induces the formation of a 'closed' active site, but the $\alpha3$–$\alpha4$ loop that forms part of the H site has a great flexibility and can undergo conformational change to allow the binding of the hydrophobic substrate. Conversely, it is conceivable that the binding of a hydrophobic substrate at the H site may induce conformational changes of the H and G sites, leading to the formation of a 'closed' active site which, however, has a great flexibility and can undergo conformational changes at the G and/or H sites to allow the binding of GSH. The crystal structure of hGSTk in complex with CDNB will eventually resolve this issue.

It has been shown previously that several classes of the dimeric soluble GSTs (including the Alpha, Mu, Pi and Delta classes) exhibit a positive co-operativity between the two active sites upon GSH binding [47–50]. These soluble GSTs contain an aromatic residue in the connecting loop between $\alpha2$ and $\beta3$ at the active site. This aromatic residue forms interactions with several hydrophobic residues of the adjacent subunit and acts as a hydrophobic lock in the dimerization, and thus plays a pivotal role in the co-operative work of the two active sites. For hGSTk, the kinetic data of both wild-type and mutant enzymes fit well with the Michealis–Menten equation and the regression coefficients of the plots are all greater than 0.95 at a variety of substrate concentrations (Tables 2, 3 and 4), which are consistent with the previous studies of rGSTk [31]. These results indicate that the two active sites of the dimeric hGSTk do not display co-operativity for both GSH and CDNB. On the other hand, the structures of hGSTk show that the G site of hGSTk is formed by structural elements of both subunits and several conserved residues of both subunits provide the interactions for the specific recognition of GSH (Figures 1A and 1B). In particular, the interactions responsible for stabilization of the $\gamma$-glutamyl and glycyl carboxylates of GSH in one subunit involve two positively charged residues ($Lys^{62'}$ and $Arg^{202'}$) of the adjacent subunit. This is different from the soluble GSTs in which the G site is located in a cleft between domain I of one subunit and domain II of the other subunit, but only residues of domain I provide the interactions for the specific recognition of GSH. Compared with the soluble GSTs, the two G sites of the dimeric hGSTk are much closer to each other owing to the unique domain topology and the tight dimer interface (the amino groups of the $\gamma$-glutamyls of the two GTX molecules at the adjacent G sites are only 5.5 Å apart) (Figure 2B). A similar case is observed in rGSTk [31]. Taken together, these results demonstrate that the two active sites of hGSTk are connected, but do not exhibit co-operativity for the substrate binding.

GSTks exist widely in the mitochondria of a variety of species ranging from bacteria to mammals. Sequence alignment of GSTks from different species indicates that the residues forming the G site and the residues interacting with GSH are highly conserved in all GSTks, including $Ser^{16}$ that interacts with the sulfur of the thiol group of GSH and functions as the catalytic residue; $Asp^{69}$, $Ser^{200}$, $Asp^{201}$ and $Arg^{202}$ that are involved in interactions with the $\gamma$-glutamyl moiety of GSH; and $Asn^{53}$, $Pro^{56}$ and $Lys^{62}$ that are involved in interactions with the glycyl moiety of GSH (Figure 1D). In addition, the $\alpha2$–$\alpha3$ connecting loop that undergoes conformational change upon substrate binding is also highly conserved in GSTks. On the other hand, the residues involved in hydrophobic substrate binding are less conserved among different GSTks, even between human and rodent GSTks (Figure 1D). Nevertheless, the structural elements forming the H site and the shape of the H site appear to be comparable in human and rat GSTks. In addition, HCCA (2-hydroxychromene-2-carboxylic acid) isomerase, a key enzyme in the naphthalene catabolic pathway of *Pseudomonas putida* which is suggested to function as a GSTk [27], has a similar overall structure and catalytic active site as hGSTk, even though the two enzymes share a low sequence identity of approximately 20 % (results not shown). The G and H sites of HCCA isomerase are also comparable with those of hGSTk and undergo conformational

changes upon substrate binding [27]. From an evolutionary perspective, variation of the residues forming the H site in GSTks from different species might confer the varied selectivity of the enzymes for a wide range of substrates and/or different enzymatic activities towards the same substrate depending on the environment to reach a better balance between the detrimental and beneficial effects of the enzymes. Taken together, it is very likely that the other GSTks might utilize a similar catalytic mechanism as that of hGSTk.

## AUTHOR CONTRIBUTION

Bing Wang carried out the structural and biochemical studies and drafted the paper. Yingjie Peng and Tianlong Zhang participated in the structural studies. Jianping Ding conceived the study, participated in the experimental design, and wrote the paper.

## ACKNOWLEDGEMENTS

We thank the staff members at the Shanghai Synchrotron Radiation Facility, Shanghai, China, for support in diffraction data collection, Professor Bin Xu at Shanghai University for providing GSDNB, and other members of our group for helpful discussion.

## FUNDING

This work was supported by the Ministry of Science and Technology of China [grant numbers 2011CB911102, 2011CB966301]; the National Natural Science Foundation of China [grant number 30730028]; the Chinese Academy of Sciences [grant number SIBS2008002]; and the Science and Technology Commission of Shanghai Municipality [grant number 10JC1416500].

## REFERENCES

1 Armstrong, R. N. (1997) Structure, catalytic mechanism, and evolution of the glutathione transferases. Chem. Res. Toxicol. **10**, 2–18
2 Oakley, A. J. (2005) Glutathione transferases: new functions. Curr. Opin. Struct. Biol. **15**, 716–723
3 Frova, C. (2006) Glutathione transferases in the genomics era: new insights and perspectives. Biomol. Eng. **23**, 149–169
4 Hayes, J. D., Flanagan, J. U. and Jowsey, I. R. (2005) Glutathione transferases. Annu. Rev. Pharmacol. Toxicol. **45**, 51–88
5 Nebert, D. W. and Vasiliou, V. (2004) Analysis of the glutathione S-transferase (GST) gene family. Hum. Genomics **1**, 460–464
6 Sheehan, D., Meade, G., Foley, V. M. and Dowd, C. A. (2001) Structure, function and evolution of glutathione transferases: implications for classification of non-mammalian members of an ancient enzyme superfamily. Biochem. J. **360**, 1–16
7 Mannervik, B., Board, P. G., Hayes, J. D., Listowsky, I. and Pearson, W. R. (2005) Nomenclature for mammalian soluble glutathione transferases. Methods Enzymol. **401**, 1–8
8 Allocati, N., Federici, L., Masulli, M. and Di Ilio, C. (2009) Glutathione transferases in bacteria. FEBS J. **276**, 58–75
9 Adler, V., Yin, Z., Fuchs, S. Y., Benezra, M., Rosario, L., Tew, K. D., Pincus, M. R., Sardana, M., Henderson, C. J., Wolf, C. R. et al. (1999) Regulation of JNK signaling by GSTp. EMBO J. **18**, 1321–1334
10 Cho, S. G., Lee, Y.H, Park, H. S., Ryoo, K., Kang, K. W., Park, J., Eom, S. J., Kim, M. J., Chang, T. S., Choi, S. Y. et al. (2001) Glutathione S-transferase mu modulates the stress-activated signals by suppressing apoptosis signal-regulating kinase 1. J. Biol. Chem. **276**, 12749–12755
11 Johansson, A. S. and Mannervik, B. (2001) Human glutathione transferase A3-3, a highly efficient catalyst of double-bond isomerization in the biosynthetic pathway of steroid hormones. J. Biol. Chem. **276**, 33061–33065
12 Li, Y. J., Oliveira, S. A., Xu, P., Martin, E. R., Stenger, J. E., Scherzer, C. R., Hauser, M. A., Scott, W. K., Small, G. W., Nance, M. A. et al. (2003) Glutathione S-transferase omega-1 modifies age-at-onset of Alzheimer disease and Parkinson disease. Hum. Mol. Genet. **12**, 3259–3267
13 Pedersen, J. Z., De Maria, F., Turella, P., Federici, G., Mattei, M., Fabrini, R., Dawood, K. F., Massimi, M., Caccuri, A. M. and Ricci, G. (2007) Glutathione transferases sequester toxic dinitrosyl-iron complexes in cells: a protection mechanism against excess nitric oxide. J. Biol. Chem. **282**, 6364–6371
14 Singh, N., Sinha, N., Kumar, S., Pandey, C. M. and Agrawal, S. (2011) Glutathione S-transferase gene polymorphism as a susceptibility factor for acute myocardial infarction and smoking in the north Indian population. Cardiology **118**, 16–21
15 Hamed, R. R., Maharem, T. M., Abdel-Meguid, N., Sabry, G. M., Abdalla, A. M. and Guneidy, R. A. (2011) Purification and biochemical characterization of glutathione S-transferase from Down syndrome and normal children erythrocytes: a comparative study. Res. Dev. Disabil. **32**, 1470–1482
16 Vasieva, O. (2011) The many faces of glutathione transferase pi. Curr. Mol. Med. **11**, 129–139
17 Dourado, D. F., Fernandes, P. A., Mannervik, B. and Ramos, M. J. (2008) Glutathione transferase: new model for glutathione activation. Chemistry **14**, 9591–9598
18 Armstrong, R. N., Rife, C. and Wang, Z. (2001) Structure, mechanism and evolution of thiol transferases. Chem.-Biol. Interact. **133**, 167–169
19 Caccuri, A. M., Antonini, G., Nicotra, M., Battistoni, A., Lo Bello, M., Board, P. G., Parker, M. W. and Ricci, G. (1997) Catalytic mechanism and role of hydroxyl residues in the active site of theta class glutathione S-transferases: investigation of Ser-9 and Tyr-113 in a glutathione S-transferase from the Australian sheep blowfly, *Lucilia cuprina*. J. Biol. Chem. **272**, 29681–29686
20 Caccuri, A. M., Antonini, G., Board, P. G., Parker, M. W., Nicotra, M., Lo Bello, M., Federici, G. and Ricci, G. (1999) Proton release on binding of glutathione to Alpha, Mu and Delta class glutathione transferases. Biochem. J. **344**, 419–425
21 Kolm, R. H., Sroga, G. E. and Mannervik, B. (1992) Participation of the phenolic hydroxyl group of Tyr-8 in the catalytic mechanism of human glutathione transferase P1-1. Biochem. J. **285**, 537–540
22 Allardyce, C. S., McDonagh, P. D., Lian, L. Y., Wolf, C. R. and Roberts, G. C. (1999) The role of tyrosine-9 and the C-terminal helix in the catalytic mechanism of Alpha-class glutathione S-transferases. Biochem. J. **343**, 525–531
23 Atkinson, H. J. and Babbitt, P. C. (2009) Glutathione transferases are structural and functional outliers in the thioredoxin fold. Biochemistry **48**, 11108–11116
24 Gustafsson, A., Pettersson, P. L., Grehn, L., Jemth, P. and Mannervik, B. (2001) Role of the glutamyl alpha-carboxylate of the substrate glutathione in the catalytic mechanism of human glutathione transferase A1-1. Biochemistry **40**, 15835–15845
25 Winayanuwattikun, P. and Ketterman, A. J. (2005) An electron-sharing network involved in the catalytic mechanism is functionally conserved in different glutathione transferase classes. J. Biol. Chem. **280**, 31776–31782
26 Jowsey, I. R., Thomson, R. E., Orton, T. C., Elcombe, C. R. and Hayes, J. D. (2003) Biochemical and genetic characterization of a murine class Kappa glutathione S-transferase. Biochem. J. **373**, 559–569
27 Thompson, L. C., Ladner, J. E., Codreanu, S. G., Harp, J., Gilliland, G. L. and Armstrong, R. N. (2007) 2-Hydroxychromene-2-carboxylic acid isomerase: a kappa class glutathione transferase from *Pseudomonas putida*. Biochemistry **46**, 6710–6722
28 Pemble, S. E., Wardle, A. F. and Taylor, J. B. (1996) Glutathione S-transferase class Kappa: characterization by the cloning of rat mitochondrial GST and identification of a human homologue. Biochem. J. **319**, 749–754
29 Robinson, A., Huttley, G. A., Booth, H. S. and Board, P. G. (2004) Modelling and bioinformatics studies of the human Kappa-class glutathione transferase predict a novel third glutathione transferase family with similarity to prokaryotic 2-hydroxychromene-2-carboxylate isomerases. Biochem. J. **379**, 541–552
30 Morel, F., Rauch, C., Petit, E., Piton, A., Theret, N., Coles, B. and Guillouzo, A. (2004) Gene and protein characterization of the human glutathione S-transferase kappa and evidence for a peroxisomal localization. J. Biol. Chem. **279**, 16246–16253
31 Ladner, J. E., Parsons, J. F., Rife, C. L., Gilliland, G. L. and Armstrong, R. N. (2004) Parallel evolutionary pathways for glutathione transferases: structure and mechanism of the mitochondrial class kappa enzyme rGSTK1-1. Biochemistry **43**, 352–361
32 Liu, M., Zhou, L., Xu, A., Lam, K. S., Wetzel, M. D., Xiang, R., Zhang, J., Xin, X., Dong, L. Q. and Liu, F. (2008) A disulfide-bond A oxidoreductase-like protein (DsbA-L) regulates adiponectin multimerization. Proc. Natl. Acad. Sci. U.S.A. **105**, 18302–18307
33 Inaba, K., Murakami, S., Suzuki, M., Nakagawa, A., Yamashita, E., Okada, K. and Ito, K. (2006) Crystal structure of the DsbB-DsbA complex reveals a mechanism of disulfide bond generation. Cell **127**, 789–801
34 Ito, K. and Inaba, K. (2008) The disulfide bond formation (Dsb) system. Curr. Opin. Struct. Biol. **18**, 450–458
35 Li, J., Xia, Z. and Ding, J. (2005) Thioredoxin-like domain of human kappa class glutathione transferase reveals sequence homology and structure similarity to the theta class enzyme. Protein Sci. **14**, 2361–2369
36 Otwinowski, Z. and Minor, W. (1997) Processing of X-ray diffraction data collected in oscillation mode. Methods Enzymol. **276**, 307–326

37 Vagin, A. and Teplyakov, A. (2010) Molecular replacement with MOLREP. Acta Crystallogr. Sect. D Biol. Crystallogr. **66**, 22–25
38 Brunger, A. T. (2007) Version 1.2 of the Crystallography and NMR system. Nat. Protoc. **2**, 2728–2733
39 Adams, P. D., Grosse-Kunstleve, R. W., Hung, L. W., Ioerger, T. R., McCoy, A. J., Moriarty, N. W., Read, R. J., Sacchettini, J. C., Sauter, N. K. and Terwilliger, T. C. (2002) PHENIX: building new software for automated crystallographic structure determination. Acta Crystallogr. Sect. D Biol. Crystallogr. **58**, 1948–1954
40 Emsley, P. and Cowtan, K. (2004) Coot: model-building tools for molecular graphics. Acta Crystallogr. Sect. D Biol. Crystallogr. **60**, 2126–2132
41 Laskowski, R. A., MacArthur, M. W., Moss, D. S. and Thornton, J. M. (1993) PROCHECK: a program to check the stereochemical quality of protein structures. J. Appl. Crystallogr. **26**, 283–291
42 Tang, S. S. and Chang, G. G. (1995) Steady-state kinetics and chemical mechanism of octopus hepatopancreatic glutathione transferase. Biochem. J. **309**, 347–353
43 Axarli, I., Dhavala, P., Papageorgiou, A. C. and Labrou, N. E. (2009) Crystal structure of *Glycine max* glutathione transferase in complex with glutathione: investigation of the mechanism operating by the Tau class glutathione transferases. Biochem. J. **422**, 247–256
44 Segel, I. H. (1975) Enzyme Kinetics: Behavior and Analysis of Rapid Equilibrium and Steady-State Enzyme Systems, pp. 560–664, John Wiley and Sons, New York
45 Allocati, N., Casalone, E., Masulli, M., Ceccarelli, I., Carletti, E., Parker, M. W. and Di Ilio, C. (1999) Functional analysis of the evolutionarily conserved proline 53 residue in *Proteus mirabilis* glutathione transferase B1-1. FEBS Lett. **445**, 347–350
46 Nathaniel, C., Wallace, L. A., Burke, J. and Dirr, H. W. (2003) The role of an evolutionarily conserved *cis*-proline in the thioredoxin-like domain of human class Alpha glutathione transferase A1-1. Biochem. J. **372**, 241–246
47 Vararattanavech, A. and Ketterman, A. J. (2007) A functionally conserved basic residue in glutathione transferases interacts with the glycine moiety of glutathione and is pivotal for enzyme catalysis. Biochem. J. **406**, 247–256
48 Oakley, A. J., Lo Bello, M., Ricci, G., Federici, G. and Parker, M. W. (1998) Evidence for an induced-fit mechanism operating in pi class glutathione transferases. Biochemistry **37**, 9912–9917
49 Ricci, G., Lo Bello, M., Caccurri, A. M., Pastore, A., Nuccetelli, M., Parker, M. W. and Federici, G. (1995) Site-directed mutagenesis of human glutathione transferase P1-1: mutation of Cys-47 induces a positive cooperativity in glutathione transferase P1-1. J. Biol. Chem. **270**, 1243–1248
50 Ricci, G., Caccuri, A. M., Lo Bello, M., Rosato, N., Mei, G., Nicotra, M., Chiessi, E., Mazzetti, A. P. and Federici, G. (1996) Structural flexibility modulates the activity of human glutathione transferase P1-1: role of helix 2 flexibility in the catalytic mechanism. J. Biol. Chem. **271**, 16187–16192
51 Gouet, P., Courcelle, E., Stuart, D. I. and Metoz, F. (1999) ESPript: analysis of multiple sequence alignments in PostScript. Bioinformatics **15**, 305–308

Received 28 April 2011/28 June 2011; accepted 28 June 2011
Published as BJ Immediate Publication 28 June 2011, doi:10.1042/BJ20110753